2019 IEEE Radio & Wireless Week

Final Program

RWW 2019

Orlando, FL USA

Rosen Plaza Hotel

20-23 January, 2019

RWW & RWS General Chair:
Rashaunda Henderson, University of Texas at Dallas

RWW & RWS General Co-Chair:
Robert Caverly, Villanova University

RWS, PAWR, WiSNet, TWIoS Technical Program Chair:
Nuno Borges Carvalho, Universidade de Aveiro

RWW Finance Chair:
Kevin Chuang, NanoSemi, Inc.

TWIoS Conference Co-Chairs:
Charlie Jackson, Northrop Grumman

Holger Maune, TU Darmstadt

PAWR Conference Co-Chairs:
Neil Braithwaite, Tarana Wireless

Pere L. Gilabert, Universitat Politècnica de Catalunya

SiRF Conference Chair:
Monte Miller, NXP Semiconductors

SiRF Technical Program Co-Chairs:
Ahmet Cagri Ulusoy, Michigan State University

Vadim Issakov, Infineon Technologies

WiSNet Conference Co-Chairs:
Rahul Khanna, Intel

Luca Roselli, University of Perugia

RWW Publications Co-Chairs:
Spyridon Pavlidis, North Carolina State University

Wasif Khan, Lahore University of Management Sciences

Aida Vera, Intel

Roberto Gomez-Garcia, University of Alcala

2019 Radio & Wireless Week Sponsor:

IEEE Microwave Theory and Techniques Society (MTT-S)

IEEE Antennas and Propagation Society (AP-S)

IEEE Aerospace and Electronic Systems Society (AESS)

http://www.radiowirelessweek.org

TUESDAY, 22 JANUARY 2019

RWS Session: TU4A

Late News Session I

Chair: José-María Muñoz-Ferreras, *University of Alcalá*
Co-Chair: Nuno Borges Carvalho, *Universidade de Aveiro*

Room: Salon 6

RWS Session: TU4B

Novel Resonator and Filter Designs

Chair: Roberto Gómez-García, *University of Alcalá*
Co-Chair: Dimitra Psychogiou, *University of Colorado Boulder*

Room: Salon 5

RWS Session: TU4C

High Performance Device Modeling and Demonstrations

Chair: Robert Caverly, *Villanova University*
Co-Chair: Peter Aaen, *University of Surrey*

Room: Salons 3/4

SiRF Session: TU4D

Frequency Synthesis

Chair:Vadim Issakov, *Infineon Technologies AG*
Co-Chair: Dietmar Kissinger, *IHP*

Room: Salons 7/8

15:40

TU4A-1 A Low Phase Noise, Wide Tuning Range 20 GHz Magnetic-Coupled Hartley-VCO in a 28 nm CMOS Technology

D. Reiter[1,2], H. Li[1], H. Knapp[1], J. Kammerer[1], S. Majied[1], B. Sene[1,2], N. Pohl[2,3], [1]Infineon Technologies AG, Neubiberg, Germany, [2]Ruhr-Universität Bochum, Bochum, Germany, [3]Fraunhofer FHR, Wachtberg, Germany

TU4B-1 Input-Reflectionless Out-of-Phase 3-dB Bandpass Filtering Couplers (Invited)

R. Gómez-García[1], J.-M. Muñoz-Ferreras[1], D. Psychogiou[2], [1]University of Alcalá, Alcalá de Henares, Spain, [2]University of Colorado Boulder, Boulder, CO, United States

TU4C-1 Transmission Experiments for 32APSK by Digital Pre-Distortion over Satellite Simulator

M. Kojima[1], Y. Suzuki[2], Y. Koizumi[1], H. Sujikai[2], [1]NHK Japan Broadcasting Corporation, Tokyo, Japan, [2]NHK Science & Technology Research Laboratories, Tokyo, Japan

TU4D-1 Chip-Scale Molecular Clock: Towards Ultra-High Frequency Stability on Low-Cost CMOS Systems (Invited)

R. Han, Massachusetts Institute of Technology, Cambridge, MA, United States

16:00

TU4A-2 A Novel Dual-Band Negative Group Delay Microwave Circuit

T. Shao, S. Fang, Z. Wang, H. Liu, S. Fu, Dalian Maritime University, Dalian, P.R. China

TU4B-2 Substrate-Integrated Waveguide Impedance Matching Network with Bandpass Filtering

J. Jeong[1], P. Kim[1], P. Pech[1], Y. Jeong[1], S. Lee[2], [1]Chonbuk National University, Jeonju, South Korea, [2]Wavice Inc., Hwaseong, South Korea

TU4C-2 Circuit Simulation Model Including Surface Effects in RF Switching PIN Diodes

R. Caverly, B. Stephanson, Villanova University, Villanova, PA, United States

16:20

TU4A-3 Linearization of BJTs with Logarithmic Predistortion

O. P. Lunden, T. Paldanius, Tampere University of Technology, Tampere, Finland

TU4B-3 Split-Distributed Resonators and Filters

S. Bulja, D. Kozlov, Nokia Bell Labs, Dublin, Ireland

TU4C-3 A 212-GHz Differential VCO with 5.3% DC-to-RF Efficiency in 65-nm CMOS Technology

X. Liu, H. Wang, J. Chen, J. Do, University of California Davis, Davis, CA, United States

TU4D-2 A Compact 3.9-4.7 GHz, 0.82 mW All-Digital PLL with 543 Fs RMS Jitter in 28 nm CMOS

R. Levinger, E. Shumaker, R. Levi, N. Machluf, S. Levin, A. Farber, G. Horovitz, Intel Corporation, Petch-Tikva, Israel

16:40

TU4A-4 An Efficient TCAD Model for TeraFET Detectors

X. Liu, M. Shur, Rensselaer Polytechnic Institute, Troy, NY, United States

TU4B-4 A New Reconfigurable Bandpass Filter With Adaptive Resonators for Switchable Passband and In-Band Notch

R. Zhang, W. Yang, D. Peroulis, Purdue University, West Lafayette, IN, United States

TU4C-4 A Compact Multi Transmission Zero Dual-Passband Filter Using Dual Stepped Impedance Resonators

T.-C. Tai[1], K.-J. Lin[2], Y.-W. Wu[1], Y.-K. Su[1], Y.-H. Wang[1], [1]National Cheng Kung University Taiwan, Tainan City, Taiwan, [2]Kun Shan University, Tainan City, Taiwan

TU4D-3 LC Tank Differential Inductor-Coupled Dual-Core 60 GHz Push-Push VCO in 45 nm RF-SOI CMOS Technology

J. Rimmelspacher[1,2], R. Weigel[1], A. Hagelauer[1], V. Issakov[2], [1]Friedrich-Alexander University Erlangen-Nuremberg, Erlangen, Germany, [2]Infineon Technologies AG, Neubiberg, Germany

17:00

TU4A-5 Adaptive Communications with Swarm Aperture

M. Hedayati[1], J. Diao[2], Y. Wang[1], [1]University of California Los Angeles, Los Angeles, CA, United States, [2]Brigham Young University, Provo, UT, United States

TU4B-5 Two Topologies of Balanced Dual-Band Bandpass Filters with Extended Common-Mode-Suppression Bandwidth

R. Gómez-García[1], J.-M. Muñoz-Ferreras[1], W. Feng[2], D. Psychogiou[3] [1]University of Alcalá, Alcalá de Henares, Spain, [2]Nanjing University of Science and Technology, Nanjing, P.R. China, [3]University of Colorado Boulder, Boulder, CO, United States

TU4C-5 Functional Performance of a Millimeter Wave Square Holey Dielectric Waveguide

D. MacFarlane[1], R. Henderson[2], K. K. O [2], M. Gomez[2], N. Aflakian[1], C. Miller[2], [1]Southern Methodist University, Dallas, TX, United States, [2]University of Texas at Dallas, Dallas, TX, United States,

TU4D-4 A 28 GHz Static CML Frequency Divider with Back-Gate Tuning on 22-Nm CMOS FD-SOI Technology

M. Hietanen, J. P. Aikio, R. Akbar, T. Rahkonen, A. Pärssinen, University of Oulu, Oulu, Finland

Substrate-Integrated Waveguide Impedance Matching Network with Bandpass Filtering

Junhyung Jeong[1], Phirun Kim[1], Phanam Pech[1], Yongchae Jeong[1], and Sangmin Lee[2]

[1]Division of Electronics and Information Engineering, Chonbuk National University, Korea
[2]Wavice Inc., Hwasung-si, Republic of Korea

***Abstract*—A substrate-integrated waveguide (SIW) impedance matching network with bandpass filtering response is proposed in this paper. The first and last *J*-inverters are affected by the termination impedances and its effect is proportional to the input or output external quality factors of the SIW filter. For validation of the proposed analysis, three-stage SIW impedance matching network with the 20-50 Ω termination impedances is designed at center frequency (f_0) of 8 GHz. The measured insertion loss is better than 0.9 dB at f_0 and better than 1.3 dB from 7.62 to 8.31 GHz (FBW = 8.6%). The measurement results are in good agreement with the simulation results.**

***Index Terms*—Bandpass filter, impedance matching, substrate-integrated waveguide.**

I. Introduction

The substrate-integrated waveguide (SIW) impedance matching network with bandpass filtering response is very useful for modern wireless communication systems to reduce a complexity, low insertion loss, low cost, small circuit size, and high-power handling. The general SIW bandpass filters (BPFs) were analyzed and designed with equal termination impedance [1-5]. In [1], the fourth-order hybrid non-uniform-Q filter with SIW and microstrip elements was proposed in the same substrate. The hybrid SIW BPF could provide an improvement of the passband flatness. In [2], a negative coupling structure SIW were proposed to improve selectivity characteristics by loading pair of transmission zeros close to the passband. Moreover, the multiple transmission zeros generated by the nonphysical cross-coupling of high order modes were proposed to improve the higher stopband performance [3]. On the other hand, the SIW BPF with partially air-filled cavity resonator was designed in [4]. Since the resonance frequency of the first cavity modes can be controlled, the high selectivity and stopband performance could be improved. In [5], even-order Chebyshev response SIW BPF was analyzed at mmW using magnetic and electric coupling. Although the high selectivity and wide stopband could be obtained in the previous works, the source and load termination impedances are equal (i.e. 50 Ω). In [6], the stepped impedance transformer SIWs were proposed in the multi-layer substrate. However, the stopband attenuation and insertion loss were poor.

In this paper, the SIW impedance matching with bandpass filtering response is proposed. The source and load termination impedances can be terminated arbitrary real impedances and proved a good stopband performance.

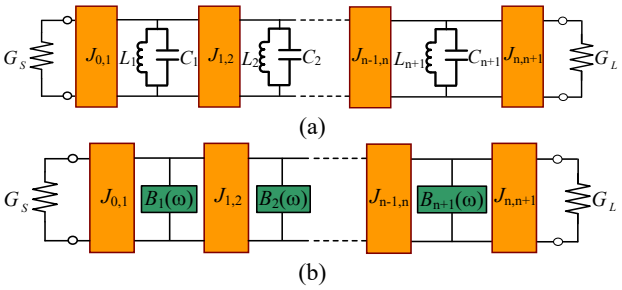

Fig. 1. Topologies of bandpass filter with admittance inverters.

II. Design Theory

Fig. 1 (a) shows topology of BPF with parallel LC resonators and admittance inverters. In practical, the shunt LC resonators can be constructed in various forms, such as transmission line (TL) resonators, waveguide resonators, or SIW resonators [7]. For generalized networks, the shunt resonators are written with the specified susceptance as seem in Fig. 1(b). As can seem in Fig. 1, the BPF is terminated with conductance source (G_S) and conductance load (G_L), respectively. Then, the generalized *J*-inverters of the BPF with admittance inverters can be expressed as (1).

$$J_{0,1} = \sqrt{\frac{G_S \mathrm{FBW} b_1}{g_0 g_1}} = \sqrt{\frac{G_S \mathrm{FBW} \omega_0 C_1}{g_0 g_1}} \tag{1a}$$

$$J_{i,i+1} = \mathrm{FBW}\sqrt{\frac{b_i b_{i+1}}{g_i g_{i+1}}} = \mathrm{FBW}\,\omega_0\sqrt{\frac{C_i C_{i+1}}{g_i g_{i+1}}} \tag{1a}$$

$$J_{n,n+1} = \sqrt{\frac{\mathrm{FBW} b_n G_L}{g_n g_{n+1}}} = \sqrt{\frac{\mathrm{FBW}\,\omega_0 C_n G_L}{g_n g_{n+1}}}\,, \tag{1a}$$

where g_0, g_1, ⋯, and g_{n+1} are the low-pass prototype element values, which can be defined for either Chebyshev or Butterworth responses, and FBW is a fractional bandwidth of the passband. $G_{S,L} = 1 / R_{S,L}$ is the conductance source and load termination conductances. As can be seem in equations (1), the first and last *J*-inverter are strongly affected by the source and load termination conductances, respectively.

For demonstration, the lossless elements are used to simulate the proposed impedance matching network using

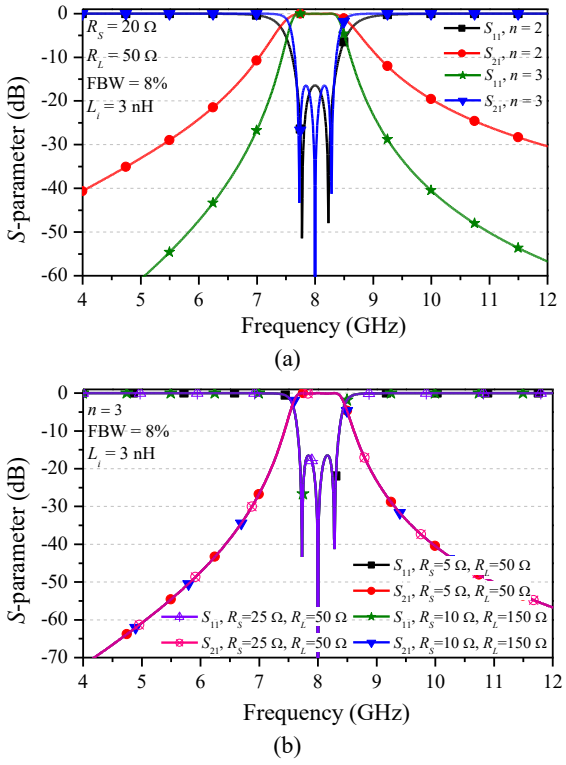

Fig. 2. *S*-parameter characteristics of proposed SIW impedance matching network with different (a) n and (b) termination impedances.

TABLE I
CALCULATED J-INVERTERS WITH DIFFERENT OF TERMINATION IMPEDANCES AND NUMBERS OF STAGE

Ripple = 0.1 dB, FBW = 8%, L_i = 3 nH, C_i = 0.13 pF					
R_S/R_L [Ω]	$J_{0,1}$	$J_{1,2}$	$J_{2,3}$	$J_{3,4}$	stages
5/50	0.010142	0.000488	0.000488	0.003207	3
10/150	0.008815	0.000488	0.000488	0.002787	
20/50	0.005071	0.000488	0.000488	0.003207	
20/50	0.005609	0.000732	0.003547		2

ADS. Fig. 2(a) and 2(b) shows the *S*-parameter characteristics of the proposed SIW impedance matching network with different numbers of stage and termination impedances, respectively. The stopband attenuation is improved as *n* increases, but the passband is maintained with different termination impedances. Although the source and load termination impedances are unequal, the passband performance can be maintained. The calculation and specifications of Fig. 2 are listed in Table I.

Fig. 3 shows the coupling mechanism of the SIW impedance matching network with bandpass filtering response, where *S* and *L* stand for source and load terminations, respectively. Moreover, Q_{eS} and Q_{eL} are the external quality factor at the source and load, respectively. r_1 to r_n are the resonators.

Fig. 3. Coupling mechanism of proposed SIW impedance matching network with bandpass filtering.

$K_{i,i+1}$ is the coupling coefficient between *i*-th and *i*+1-th resonators.

From [7], the design parameters can be obtained as (2).

$$Q_{eS} = \frac{b_1}{J_{0,1}^2 R_S} = \frac{C_1 \omega_0}{J_{0,1}^2 R_S} \tag{2a}$$

$$K_{i,i+1} = \frac{J_{i,i+1}}{\sqrt{b_i b_{i+1}}} = \frac{J_{i,i+1}}{\omega_0 \sqrt{C_i C_{i+1}}} \tag{2b}$$

$$Q_{eL} = \frac{b_n}{J_{n,n+1}^2 R_L} = \frac{C_n \omega_0}{J_{n,n+1}^2 R_L} \tag{2c}$$

In practical SIW impedance matching network, the $Q_{eS,eL}$ and $K_{i,i+1}$ can be obtained from the electromagnetic (EM) simulation by the following equation [7].

$$Q_{eS,eL} = \frac{f_0}{\Delta f_{\pm 3\text{dB}}}, \tag{3}$$

where f_0 is the center frequency and $\Delta f_{\pm 3\ \text{dB}}$ is the 3-dB bandwidth. Similarly, the coupling coefficient between two resonators (K_{12} and $K_{n,n+1}$) can be extracted from the EM simulation by using (4) for asynchronous case.

$$K_{1,2} = K_{n-1,n} = \pm \frac{1}{2}\left(\frac{f_{R_1}}{f_{R_2}} + \frac{f_{R_2}}{f_{R_1}}\right)\sqrt{\left(\frac{f_{p_2}^2 - f_{p_1}^2}{f_{p_2}^2 + f_{p_1}^2}\right)^2 - \left(\frac{f_{R_2}^2 - f_{R_1}^2}{f_{R_2}^2 + f_{R_1}^2}\right)^2}, \tag{4}$$

where f_{Rj} (j = 1, 2) is the self-resonance frequency and f_{pj} is the two split resonant frequencies. Thereafter, the coupling coefficient between two intermediate resonators can be extracted from the EM simulation by using (5) for synchronously tuned coupled resonators.

$$K_{i,i+1} = \pm \frac{f_{p2}^2 - f_{p1}^2}{f_{p2}^2 + f_{p1}^2}, \tag{5}$$

where *i* is start from 2 to n-1.

III. SIMULATION AND MEASUREMENT

For the experimental verification, the proposed SIW impedance matching network was designed to operate at f_0 of 8 GHz with 0.1 dB passband ripple, FBW = 8%, R_S = 20 Ω, R_L = 50 Ω, and three-stage resonators. The calculated *J*-inverters values are listed in Table I. From (2), the external quality factors at the source and load and coupling coefficient between two resonators are found as Q_{eS} = 12.895, Q_{eL} = 5.578, and K_{12} = K_{23} = 0.0735. Using electromagnetic (EM), the Q_{eS} or Q_{eL}, and $K_{i,i+1}$ can be

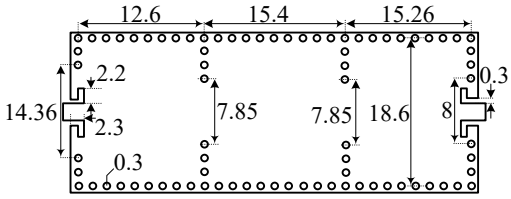

(a)

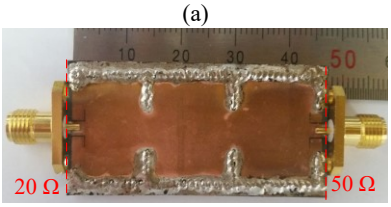

(b)

Fig. 4. Proposed SIW impedance matching network: (a) layout and (b) photograph of fabricated circuit. (unit: mm)

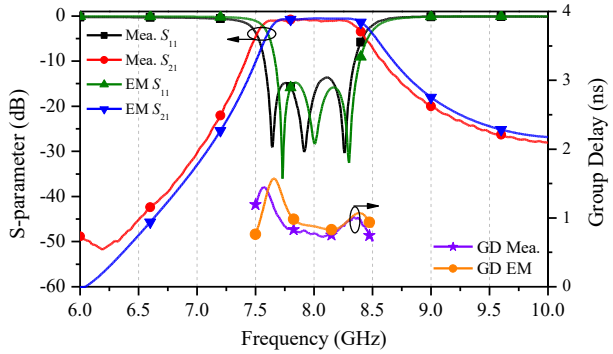

Fig. 5. Simulated and measured frequency responses of the proposed SIW impedance matching network.

extracted and calculated using (3), (4), and (5), respectively, as mentioned in [5] and [7].

The layout and photograph of fabricated SIW impedance matching network are shown in Fig. 4 with the physical dimensions. Since, the Q_{eS} and Q_{eL} are not the same for impedance matching, the input and output via-hole iris window are not the same. The filter is implemented in microstrip substrate with a RT/Duroid 5880 dielectric constant (ε_r) of 2.2 and thickness (h) of 31 mils. The overall circuit size of the fabricated network is 19.8 mm × 46.46 mm. The EM simulation was performed using Ansys HFSS. The measurement of proposed SIW impedance matching has done after TRL calibration technique and it has been mentioned in [8].

Fig. 5 shows the comparison of EM simulation and measurement results of the proposed SIW impedance matching network. The measured in-band insertion loss is better than 0.9 dB at 8 GHz and better than 1.3 dB from 7.62 to 8.31 GHz (FBW = 8.6%). The passband has been shifted 40 MHz to the low frequency. The shifted frequency might be the due to the fabrication error. The input return loss within the whole passband are better than 13.7 dB. Moreover, the attenuations at 400 MHz lower- and upper-sides of the passband are better than 15 dB. The measured group delay of the passband is lower than 0.8 ns at f_0 and better than 1.4 ns in the whole passband.

IV. Conclusion

In this paper, a new designed SIW impedance matching network with bandpass filtering response is proposed. The source and load termination impedances can be changed with arbitrary real impedance. For the validity, three-stage SIW impedance matching network is designed, simulated, and measured. The proposed SIW impedance matching is expected to be advantageous in matching network designs of power amplifier and antenna at microwave frequency.

Acknowledgment

Research reported in this work has been supported by ICMTC (Institute of Civil-Military Technology Cooperation) of Korea under an ICMTC program (16-CM-SS-16).

References

[1] L.-F. Qiu, L.-S. Wu, W.-Y. Yin, and J.-F. Mao, "Hybrid non-uniform-Q lossy filters with substrate integrated waveguide and microstrip resonators," *IET Microw. Antennas Propag.*, vol. 12, no. 1, pp. 92-98, 2018.

[2] B. Lee, S. Nam, C. Kwak, and J. Lee, "New negative coupling structure for K-band substrate-integrated waveguide resonator filter with a pair of transmission zeros," *IEEE Microw. Wireless Compon. Lett.*, vol. 28, no. 2, pp. 135-137, Feb. 2018.

[3] X.-P. Chen, K. Wu, and D. Drolet, "Substrate integrated waveguide filter with improved stopband performance for satellite ground terminal," *IEEE Microw. Wireless Compon. Lett.*, vol. 57, no. 3, pp. 674-676, Mar. 2009.

[4] C. Tomassoni, L. Silvestri, A. Ghiotto, M. Bozzi, and L. Perregrini, "Subtrate-integrated waveguide filters based on dual-mode air-filled resonant cavities," *IEEE Transac. Microw. Theory Techniq.*, vol. 66, no. 2, pp. 726-736, Feb. 2018.

[5] K. Wang, S.-W. Wong, G.-H. Sun, Z. Chen, L. Zhu, and Q.-X. Chu, "Synthesis method for substrate-integrated waveguide bandpass filter with even-order Chebyshev response," *IEEE Transac. Compon. Packag. Manufact. Technology*, vol. 6, no. 1, pp. 126-135, Jan. 2016.

[6] T. Jaschke, B. Rohrdantz, and A. F. Jacob, "Dual-band stepped-impedance transformer to full-height substrate-integrated waveguide," *45th European Microw. Conference*, Paris, France, pp. 367–370, Sep. 2015.

[7] J.-S. Hong, *Microstrip Filters for RF/Microwave Applications.*, 2nd edition, New York, NY, USA: Wiley, 2011.

[8] P. Kim, G. Chaudhary, and Y. Jeong, "Impedance matching bandpass filter with a controllable spurious frequency based on λ/2 stepped impedance resonator," *IET Microw. Antennas Propag.*, DOI:10.1049/iet-map.2018.5127.